Time-dependent density-functional theory for real-time electronic dynamics on material surfaces

Rulin Wang,[1,2] Dong Hou,[1] and Xiao Zheng[1,*]

[1]*Hefei National Laboratory for Physical Sciences at the Microscale, University of Science and Technology of China, Hefei, Anhui 230026, China*

[2]*Department of Physics, University of Science and Technology of China, Hefei, Anhui 230026, China*

(Received 27 May 2013; revised manuscript received 16 September 2013; published 19 November 2013)

The real-time electronic dynamics on material surfaces is critically important to a variety of applications. However, their simulations have remained challenging for conventional methods such as the time-dependent density-functional theory (TDDFT) for isolated and periodic systems. By extending the applicability of TDDFT to systems with open boundaries, we achieve accurate atomistic simulations of real-time electronic response to local perturbations on material surfaces. Two prototypical scenarios are exemplified: the relaxation of an excess electron on a graphene surface and the electron transfer across the molecule-graphene interface. Both the transient and long-time asymptotic dynamics are validated, which accentuates the fundamental importance and usefulness of an open-system TDDFT approach. The simulations also provide insights into the characteristic features of temporal electron evolution and dissipation on surfaces of bulk materials.

DOI: 10.1103/PhysRevB.88.205126 PACS number(s): 71.15.Mb, 72.80.Vp, 73.20.Mf, 73.40.−c

I. INTRODUCTION

How electrons evolve at the surfaces or interfaces of materials is fundamentally significant to a variety of applications, including photovoltaics, nanoelectronics, heterogeneous catalysis, etc. Consider a prototypical system in which a molecule is adsorbed on a surface of a material. For instance, in a dye-sensitized solar cell,[1] photoexcited electrons transfer from the dye molecule to the semiconductor surface and then drain into the bulk.[2] In a biomimetic water-splitting complex, a catalytic molecule acquires electrons by oxidation of water and then feeds them into the supporting conductor.[3] Apparently, for these systems the real-time electronic processes on material surfaces are crucially important to their functionality. Accurate simulations at the atomic level will be very helpful for understanding the key features of the real-time electronic dynamics and the underlying mechanisms.

Considering the size and complexity of a system involving a material surface, the time-dependent density-functional theory (TDDFT)[4–7] is potentially suitable for carrying out the theoretical studies, due to its favorable balance between accuracy and efficiency. TDDFT has been successfully implemented in both frequency[8] and time domains.[9,10]

For practical application of TDDFT, a boundary condition should be imposed explicitly or implicitly. So far the success of TDDFT has been largely restricted to isolated and periodic boundary conditions. For isolated systems (atoms, molecules, clusters, etc.), the electron density falls off to zero at infinite distance, and the existence of a rigorous TDDFT has been proven by the Runge-Gross theorem[4] and van Leeuwen's extension.[11,12] For periodic systems (polymers, crystals, etc.), the electron density possesses the lattice translational invariance symmetry, and the rigorousness of TDDFT has been discussed by many authors.[13–18] TDDFT has been widely employed to study excited-state properties (such as absorption and electron-energy-loss spectra) of periodic solids.[19–22] The energy relaxation and dissipation in extended systems have been addressed by the time-dependent current-density-functional theory[23,24]—an extension of TDDFT with explicit inclusion of dynamical exchange-correlation effects.

Apparently, for a composite system in which a molecule is adsorbed on a material surface, neither an isolated nor a periodic model is suitable, particularly when the electronic dynamics is triggered by a local perturbation. In such a case, it is ideal to treat the molecule with the part of the surface around the adsorption site as an *open* system, while taking the rest of bulk material as the *environment*.

TDDFT for open systems has been proposed by various authors to study electron transport through molecular or nanoelectronic devices coupled to macroscopic electrodes.[25–29] With electron current flowing through a device, it is impractical or inappropriate to treat the device-electrodes composite or the device itself as either isolated or periodic. With the open-system TDDFT, the device is regarded as a system having an open boundary, while the electrodes constitute the environment which serves as electron reservoirs and energy sinks.

The open-system TDDFT can be built on a formally exact theoretical foundation.[28,30–35] In particular, the existence of a rigorous TDDFT for a general open system coupled to any large but finite environment has been proven by a time-dependent holographic electron-density theorem.[28,32,33] In principle (but unfortunately not in practice), the electron density inside the open boundary alone should suffice to determine all equilibrium and nonequilibrium properties of the entire composite system (system plus environment).[33]

Despite the progress made, application of TDDFT beyond electron transport in one-dimensional systems[36–41] has been very rare. The main difficulty is the accurate characterization of dissipative processes occurring at the designated boundary, including the energy relaxation, electron transfer, and decoherence. Meanwhile, resolving the atomistic and spectral details of the environment and addressing their influences on the open system present further challenges.

In this paper, we will (1) show how the effects of the bulk surface (environment) can be taken into account accurately and efficiently in TDDFT; (2) extend the applicability of TDDFT to simulations of real-time electronic dynamics on two-dimensional material surfaces; (3) elucidate the boundary

effects on the simulation results; and (4) highlight the fundamental importance and usefulness of the open-system model and approach.

The remainder of this paper is organized as follows. In Sec. II we summarize the time-domain TDDFT formalisms corresponding to isolated, periodic, and open boundary conditions. The characterization of dissipative interactions between an open system and its environment is elaborated. Section III presents the simulations of real-time electronic dynamics on a graphene surface and a molecule-graphene interface. Concluding remarks are finally given in Sec. IV.

II. TDDFT FORMALISMS FOR ISOLATED, PERIODIC, AND OPEN BOUNDARY CONDITIONS

For isolated systems, the Kohn-Sham equation of motion for the reduced single-electron density matrix is[10]

$$i\dot{\boldsymbol{\sigma}}(t) = [\boldsymbol{h}(t),\boldsymbol{\sigma}(t)]. \tag{1}$$

Here, $\boldsymbol{\sigma}(t)$ is the Kohn-Sham density matrix of the isolated system, and the Kohn-Sham Hamiltonian $\boldsymbol{h}(t)$ consists of the kinetic term, the external potential, the Hartree potential, and the exchange-correlation potential.

For periodic systems, we have[42]

$$i\dot{\boldsymbol{\sigma}}_{\boldsymbol{k}}(t) = [\boldsymbol{h}_{\boldsymbol{k}}(t),\boldsymbol{\sigma}_{\boldsymbol{k}}(t)], \tag{2}$$

where $\boldsymbol{k}$ is the wave vector and $\boldsymbol{\sigma}(t) = \int_{\mathrm{BZ}} \boldsymbol{\sigma}_{\boldsymbol{k}}(t)\, d\boldsymbol{k}/\Omega_{\mathrm{BZ}}$, with Ω_{BZ} being the volume of the Brillouin zone.

For open systems, the general Kohn-Sham equation of motion has been derived as[28]

$$i\dot{\boldsymbol{\sigma}}(t) = [\boldsymbol{h}(t),\boldsymbol{\sigma}(t)] - i\,\boldsymbol{Q}(t). \tag{3}$$

Here, the dimension of matrices $\boldsymbol{\sigma}(t)$ and $\boldsymbol{h}(t)$ corresponds to the size of the open system. The matrix $\boldsymbol{Q}(t)$ addresses the dissipative processes occurring at the boundary, such as the exchanges of energy, electrons, and phase information between the open system and the environment. For instance, the total electron current flowing over the boundary at time t can be evaluated as $I(t) = -\mathrm{tr}[\boldsymbol{Q}(t)]$.[28]

The main challenge in developing a practical TDDFT method for open systems is to find an accurate and efficient scheme to compute $\boldsymbol{Q}(t)$. A number of approaches have been proposed, such as the nonequilibrium Green's-function (NEGF) method,[26,43] the adiabatic wide-band limit approximation,[28] and the perturbative master equation approach.[29,44] However, the practicality of these approaches is restrained by their respective limitations. For instance, in the TDDFT-NEGF formalism, Eq. (3) becomes an integrodifferential equation which is extremely difficult to solve.[28] The wide-band limit approximation simplifies the computation of $\boldsymbol{Q}(t)$, but the resulted electronic dynamics becomes sometimes less accurate since the energy dependence of the environment spectral function is neglected.

In recent years, a quantum dissipation theory—the hierarchical equations of motion (HEOM) theory—has been developed for general open electronic systems.[45–47] The HEOM method provides a unified approach for the characterization of equilibrium and nonequilibrium as well as static and dynamic properties.[48–53] The HEOM formalism resolves nonperturbatively the combined effects of electron-electron interaction, system-environment dissipative coupling, and non-Markovian memory. The basic variables of the HEOM are the reduced system density matrix and a number of auxiliary density matrices. For systems involving electron-electron interaction the hierarchy needs to be truncated at a certain level L. Mathematically, this can be done by setting all the auxiliary density matrices at the levels higher than L to zero. In principle, the exact solution is guaranteed at $L \to \infty$, provided that the environment satisfies the Gaussian statistics (such as for a noninteracting electron reservoir). In practice, the results usually converge rapidly with the increasing L at finite temperatures. Once the convergence is achieved, the numerical outcome is considered to be quantitatively accurate.[51]

A remarkable feature of the HEOM formalism is that, for noninteracting electronic systems, the hierarchy terminates automatically at $L = 2$, without approximation.[45] This has been verified by our previous calculations. For instance, the HEOM approach has reproduced[48] the exact time-dependent current response of a noninteracting quantum dot to step-function bias voltages.[36,54] Noting that the Kohn-Sham reference system is effectively noninteracting, it is thus ideal to integrate the HEOM approach into the framework of TDDFT. In this way, a TDDFT-HEOM approach can be developed to describe realistic open electronic systems.[55–58]

The TDDFT-HEOM formalism is formally equivalent to the TDDFT-NEGF method,[55,59] and it is numerically much more convenient than the latter. This is because the integrodifferential equation associated with the NEGF method is now replaced by a set of differential equations, which can be solved straightforwardly. The detailed derivations of the TDDFT-HEOM formalism for open electronic systems have been presented in Refs. 55 and 56. Here, we briefly summarize the formulas which are essentially relevant to our following simulations.

In the NEGF formalism,[60,61] the effects of environment are characterized by the self-energies. At equilibrium, the self-energies are

$$\begin{aligned}\tilde{\boldsymbol{\Sigma}}^{<}(t) &= i\int d\epsilon\, f_\beta(\epsilon)\boldsymbol{\Lambda}(\epsilon)\, e^{-i\epsilon t},\\ \tilde{\boldsymbol{\Sigma}}^{>}(t) &= -i\int d\epsilon\, [1 - f_\beta(\epsilon)]\boldsymbol{\Lambda}(\epsilon)\, e^{-i\epsilon t}.\end{aligned} \tag{4}$$

Here, $f_\beta(\epsilon)$ is the Fermi function with $\beta = 1/k_B T$, and $\boldsymbol{\Lambda}(\epsilon)$ is the spectral function (or linewidth) matrix of the environment.

The construction of HEOM relies on how the self-energies $\tilde{\boldsymbol{\Sigma}}^{x}(t)$ $(x = <, >)$ are expanded into exponential functions. In the context of quantum dissipation theory, this means how the memory of environment is resolved by a number of characteristic modes. Mathematically, this can be achieved by applying the contour integral technique with the residual theorem. In this way, the poles of both $f_\beta(\epsilon)$ and $\boldsymbol{\Lambda}(\epsilon)$ in the complex energy space contribute to the resulting characteristic memory modes. Details about the memory decomposition can be found in our previous works such as Refs. 45 and 46. Various schemes have been proposed for the decomposition of memory, such as the Matsubara decomposition scheme,[45] the partial fractional decomposition scheme,[62] a hybrid Matsubara

decomposition and frequency dispersion scheme,[46] and a Padé decomposition scheme.[63–65] Among all these schemes, the Padé decomposition scheme is so far the most efficient one.[47]

For the systems investigated in Sec. III of this paper, the bulk graphene plays the role of environment. To resolve the spectral function of a realistic bulk material, we use a combined Padé and Lorentzian decomposition (PLD) scheme,[55,56] which involves the following expansions:

$$f_\beta(\epsilon) = \frac{1}{e^{\beta(\epsilon-\mu)}+1} \simeq \frac{1}{2} + \sum_{p=1}^{P} \frac{R_p}{\beta}\left(\frac{1}{\epsilon-\mu-\frac{z_p^+}{\beta}} + \frac{1}{\epsilon-\mu-\frac{z_p^-}{\beta}}\right), \quad (5)$$

$$\mathbf{\Lambda}(\epsilon) \approx \sum_{d=1}^{D} \frac{1}{(\epsilon-\Omega_d)^2+W_d^2}\,\mathbf{\Lambda}_d. \quad (6)$$

Here, μ is the environment chemical potential at equilibrium. The weights $\{R_p\}$ and poles $\{z_p^\pm\}$ are determined by the Padé expansion.[64] In principle, the expansion of Eq. (5) becomes exact at $P\to\infty$. In practice, an appropriate value should be assigned to P: it must be sufficiently large to preserve the accuracy of Eq. (5), but not too large so as to reduce the computational cost for the resulting HEOM. For instance, at $T = 100\,\mathrm{K}$, a minimal $P = 20$ is required to reproduce $f_\beta(\epsilon)$ accurately. As the temperature lowers, a larger P is needed. In Eq. (6), $\{\Omega_d\}$ and $\{W_d\}$ are the centers and widths of the Lorentzian functions, and $\{\mathbf{\Lambda}_d\}$ are the coefficient matrices. They are obtained by a least-square fit to $\mathbf{\Lambda}(\epsilon)$. The Lorentzian fitting of $\mathbf{\Lambda}(\epsilon)$ is not unique, and the strategy of finding the optimal $\{\Omega_d\}$ and $\{W_d\}$ may vary from system to system.

By inserting Eqs. (5) and (6) into Eq. (4), and using the contour integral technique as well as the residue theorem, the greater and lesser self-energies are expanded as

$$\tilde{\mathbf{\Sigma}}^x(t) \simeq \sum_{m=1}^{M} \tilde{\mathbf{\Sigma}}_m^x(t) = \sum_{m=1}^{M} \boldsymbol{A}_m^{x,\sigma}\, e^{\gamma_m^\sigma t}, \quad (7)$$

with $M = P + D$ and $\sigma = \pm$. Each component of self-energy $\tilde{\mathbf{\Sigma}}_m^x(t)$ corresponds to an exponentially decaying function of $|t|$, and it is associated with the characteristic memory time $|\mathrm{Re}(\gamma_m^\sigma)|^{-1}$. The coefficients $\{\boldsymbol{A}_m^{x,\pm}\}$ and exponents $\{\gamma_m^\pm\}$ are evaluated via

$$\boldsymbol{A}_m^{<\pm} = \begin{cases} \frac{i\pi\mathbf{\Lambda}_m}{W_m} f_\beta(\Omega_m \pm i W_m) & m \leqslant D \\ \mp\frac{2\pi R_p}{\beta}\mathbf{\Lambda}\left(\mu+\frac{z_p^\pm}{\beta}\right) & m > D, p = m-D \end{cases},$$

$$\boldsymbol{A}_m^{>\pm} = \begin{cases} -\frac{i\pi\mathbf{\Lambda}_m}{W_m} \bar{f}_\beta(\Omega_m \pm i W_m) & m \leqslant D \\ \mp\frac{2\pi R_p}{\beta}\mathbf{\Lambda}\left(\mu+\frac{z_p^\pm}{\beta}\right) & m > D, p = m-D \end{cases},$$

$$\gamma_m^\pm = \begin{cases} -i\,(\Omega_m \pm i W_m) & m \leqslant D \\ -i\left(\mu+\frac{z_p^\pm}{\beta}\right) & m > D, p = m-D \end{cases}, \quad (8)$$

where $\bar{f}_\beta(\omega) \equiv 1 - f_\beta(\omega)$. Note that Eq. (7) holds only at $t > 0$ with $\sigma = -$, while it is valid only at $t < 0$ with $\sigma = +$.

Based on the PLD scheme, the TDDFT-HEOM are established as follows:

$$i\,\dot{\boldsymbol{\sigma}}(t) = [\boldsymbol{h}(t),\boldsymbol{\sigma}] - \sum_{m=1}^{M}[\boldsymbol{\varphi}_m(t) - \boldsymbol{\varphi}_m^\dagger(t)], \quad (9)$$

$$i\,\dot{\boldsymbol{\varphi}}_m(t) = [\boldsymbol{h}(t) - \Delta\mu(t) - i\gamma_m^+]\,\boldsymbol{\varphi}_m + \sum_{m'=1}^{M} \boldsymbol{\psi}_{mm'} - i[(1-\boldsymbol{\sigma})\boldsymbol{A}_m^{<+} + \boldsymbol{\sigma}\,\boldsymbol{A}_m^{>+}], \quad (10)$$

$$i\,\dot{\boldsymbol{\psi}}_{mm'}(t) = i(\gamma_{m'}^- - \gamma_m^+)\boldsymbol{\psi}_{mm'} + i(\boldsymbol{A}_{m'}^{>-} - \boldsymbol{A}_{m'}^{<-})\boldsymbol{\varphi}_m - i\boldsymbol{\varphi}_{m'}^\dagger(\boldsymbol{A}_m^{>+} - \boldsymbol{A}_m^{<+}). \quad (11)$$

The basic variables are $\{\boldsymbol{\sigma}(t),\boldsymbol{\varphi}_m(t),\boldsymbol{\psi}_{mm'}(t)\}$, and the total number of unknown matrices is $M^2 + M + 1$ with $M = P + D$. In this work, a group of Lorentzian functions with a fixed D and predesignated $\{\Omega_d, W_d\}$ is used as basis functions to approximate $\mathbf{\Lambda}(\epsilon)$ of Eq. (6), and the coefficients $\{\mathbf{\Lambda}_d\}$ are determined via a least-square fit. In this way, the positions and shapes of the Lorentzian functions can be tuned conveniently and systematically. For the systems considered in Sec. III, $M < 100$ is sufficient for achieving a reasonably accurate decomposition of $\mathbf{\Lambda}(\epsilon)$.

A residual correction approach is further applied to minimize any minor error that might come up with the PLD scheme. Note that the Kohn-Sham density matrix of an equilibrium open system $\boldsymbol{\sigma}^{\mathrm{eq}}$ can be obtained very accurately by making use of the full information of self-energies $\tilde{\mathbf{\Sigma}}^x(\epsilon)$. This can be done, for instance, by using the NEGF method[28] without having to invoke the PLD. Consequently, if the real-time dynamics of an open system starts from an equilibrium state, the time evolution of $\boldsymbol{\sigma}(t)$ can be replaced by that of $\boldsymbol{\sigma}^{\mathrm{eq}} + \Delta\boldsymbol{\sigma}(t)$, where $\Delta\boldsymbol{\sigma}(t)$ is the induced Kohn-Sham density matrix. Therefore, Eqs. (9) and (10) can be replaced by

$$i\,\Delta\dot{\boldsymbol{\sigma}}(t) = [\boldsymbol{h}(t),\boldsymbol{\sigma}^{\mathrm{eq}} + \Delta\boldsymbol{\sigma}(t)] - \sum_{m=1}^{M}[\boldsymbol{\varphi}_m(t) - \boldsymbol{\varphi}_m^\dagger(t)] - i\,\Delta\boldsymbol{Q}_0, \quad (12)$$

$$i\,\dot{\boldsymbol{\varphi}}_m(t) = [\boldsymbol{h}(t) - \Delta\mu(t) - i\gamma_m^+]\boldsymbol{\varphi}_m(t) - i[1 - \boldsymbol{\sigma}^{\mathrm{eq}} - \Delta\boldsymbol{\sigma}(t)]\boldsymbol{A}_m^{<+} - i[\boldsymbol{\sigma}^{\mathrm{eq}} + \Delta\boldsymbol{\sigma}(t)]\boldsymbol{A}_m^{>+} + \sum_{m'=1}^{M}\boldsymbol{\psi}_{mm'}(t). \quad (13)$$

Here, $\Delta\boldsymbol{Q}_0 \equiv \boldsymbol{Q}_{\mathrm{NEGF}}^{\mathrm{eq}} - \boldsymbol{Q}_{\mathrm{PLD}}^{\mathrm{eq}}$ is the residual correction term for $\boldsymbol{Q}(t)$, where $\boldsymbol{Q}_{\mathrm{NEGF}}^{\mathrm{eq}}$ is obtained from $\tilde{\mathbf{\Sigma}}^x(\epsilon)$ through a stationary-state calculation without invoking the decomposition of Eq. (7).

As we will show later in Sec. III, the residual correction approach significantly improves the accuracy of the TDDFT-HEOM approach on the real-time electronic dynamics. Moreover, it preserves the numerical efficiency of TDDFT-HEOM, and hence the TDDFT-HEOM calculation on the real-time dynamics remains much more convenient than the TDDFT-NEGF method. With the predetermined $\boldsymbol{\sigma}^{\mathrm{eq}}$ and $\Delta\boldsymbol{Q}_0$, the basic variables of TDDFT-HEOM become $\{\Delta\boldsymbol{\sigma}(t),\boldsymbol{\varphi}_m(t),\boldsymbol{\psi}_{mm'}(t)\}$, and the time evolution of an open system is now characterized by Eqs. (11)–(13).

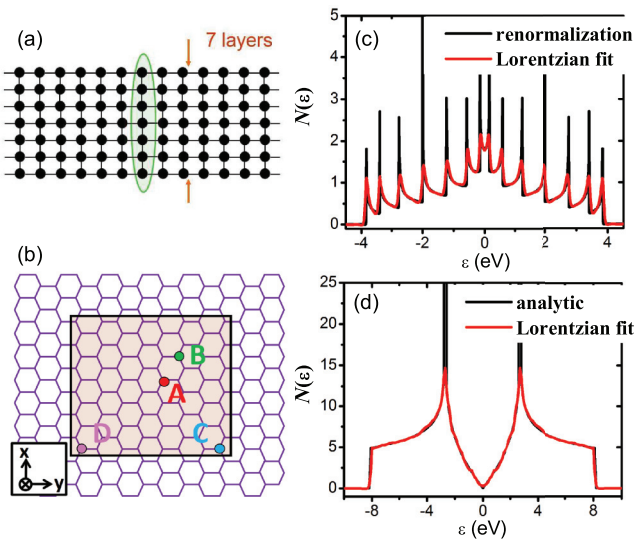

FIG. 1. (Color online) Schematic diagrams of (a) a quasi-one-dimensional atomic chain of a finite width (seven layers), where the green circle marks the open system, and (b) a two-dimensional graphene monolayer, where the atoms in the shaded area constitute the open system. (c), (d) Equilibrium PDOS computed with and without the Lorentzian fitting of Eq. (6), respectively.

III. RESULTS AND DISCUSSIONS

A. Numerical validation of the TDDFT-HEOM approach

To validate the accuracy of the TDDFT-HEOM construction based on the PLD scheme, we perform numerical tests on two prototypical systems: (1) a quasi-one-dimensional atomic chain [see Fig. 1(a)] and (2) a two-dimensional graphene monolayer [see Fig. 1(b)].

We examine the projected density of states (PDOS) of the open system (including all the atoms inside the open boundary) at equilibrium, which is computed via[66,67]

$$N(\epsilon) = -\frac{1}{\pi}\,\mathrm{Im}\{\mathrm{tr}[\epsilon \boldsymbol{I} - \boldsymbol{h} - \boldsymbol{\Gamma}(\epsilon) - i\boldsymbol{\Lambda}(\epsilon)]^{-1}\}. \qquad (14)$$

Here, $\boldsymbol{\Gamma}(\epsilon)$ is the real part of retarded self-energy $\tilde{\boldsymbol{\Sigma}}^r(\epsilon)$, which can be obtained from $\boldsymbol{\Lambda}(\epsilon)$ via the Kramers-Kronig relation.[68]

We first carry out a numerical test on the homogeneous atomic chain depicted in Fig. 1(a), where the whole chain is described by a tight-binding model. The energetic parameters are the on-site energy $\epsilon_0 = 0$ and the nearest-neighbor coupling $\gamma = 1$ eV. We choose the atoms on a cross section as the open system, and the rest of the chain is taken as the environment. Apparently, the environment consists of two semi-infinite periodic lattices, and hence its spectral function $\boldsymbol{\Lambda}(\epsilon)$ can be obtained very accurately by using a highly convergent renormalization algorithm.[69]

The construction of HEOM requires the spectral function $\boldsymbol{\Lambda}(\epsilon)$ to be decomposed into Lorentzian functions; see Eq. (6). The fitting Lorentzian functions are centered at 15 equally spaced energy points, and each center is assigned with three different widths. Therefore, the total number of Lorentzian functions used is 45, i.e., $D = 45$. The PDOS of the open system is then evaluated via Eq. (14) with and without the use of Eq. (6), and the calculated results are compared in Fig. 1(c). As shown clearly, although the line shape of $N(\epsilon)$ is somewhat complicated, the two curves agree very well with each other. The only minor deviations appear at the energies of van Hove singularities. These minor deviations do not affect the normalization of the PDOS. This thus verifies that the Lorentzian fit for $\boldsymbol{\Lambda}(\epsilon)$ is reasonably accurate.

We then move to the more challenging case of a two-dimensional graphene monolayer. Suppose the bulk graphene resides in the xy plane. A rectangular piece of graphene containing 96 atoms is chosen as the simulation box; see the shaded area in Fig. 1(b). It is to be treated explicitly by TDDFT approaches and is subjected to specific boundary conditions. The atoms on the graphene plane form a perfectly periodic two-dimensional lattice, and the C–C bond length assumes the typical value of 1.42 Å.[70] Because of the delocalized sp^2 network, conduction electrons can move easily on the (xy) plane.[71] A tight-binding Hamiltonian is used to represent the p_z electrons of all carbon atoms, with the on-site energy $\epsilon_0 = 0$ and nearest-neighbor coupling $\gamma = 2.7$ eV.[72]

We point out here that the renormalization scheme of Ref. 69 is not applicable to the evaluation of $\boldsymbol{\Lambda}(\epsilon)$ for a two-dimensional environment such as the bulk graphene. Instead, a $\boldsymbol{k}$-sampling scheme proposed in Ref. 73 is employed. This scheme involves the calculation of surface Green's functions of a bulk graphene, and these Green's functions are required to vanish properly in the open system (inside the simulation box). The self-energies and the spectral function $\boldsymbol{\Lambda}(\epsilon)$ are then obtained by collecting the surface Green's functions of all wave vectors $\boldsymbol{k}$.

Figure 2 demonstrates some diagonal and off-diagonal elements of $\boldsymbol{\Lambda}(\epsilon)$ obtained by using the $\boldsymbol{k}$-sampling technique. To construct the HEOM, we then use the same set of Lorentzian functions ($D = 45$) as that for the atomic chain to fit $\boldsymbol{\Lambda}(\epsilon)$. The fitted data are compared to the $\boldsymbol{k}$-sampling results in Fig. 2. Apparently, although the overall feature is well captured by the Lorentzian fit, there are some minor discrepancies in the detailed line shapes, particularly at energies at which the curve is rather spiky.

The PDOS of the graphene inside the simulation box is then calculated, shown in Fig. 1(d). An analytic form of the PDOS is available for the graphene described by the tight-binding Hamiltonian.[72] As shown in Fig. 1(d), the calculated PDOS with the Lorentzian fitting of $\boldsymbol{\Lambda}(\epsilon)$ agrees nicely with the analytic data. The only minor deviations occur at the van Hove singularities $\epsilon = \pm\gamma$, which are due to a finite level

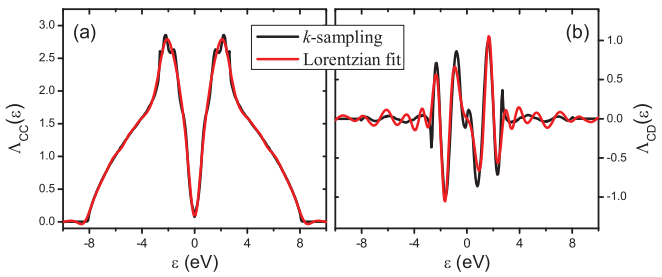

FIG. 2. (Color online) (a) A diagonal element (for atom C) and (b) an off-diagonal element (between atoms C and D) of spectral function matrix $\boldsymbol{\Lambda}(\epsilon)$ for the graphene monolayer as sketched in Fig. 1(b). The positions of atoms C and D are also marked in Fig. 1(b).

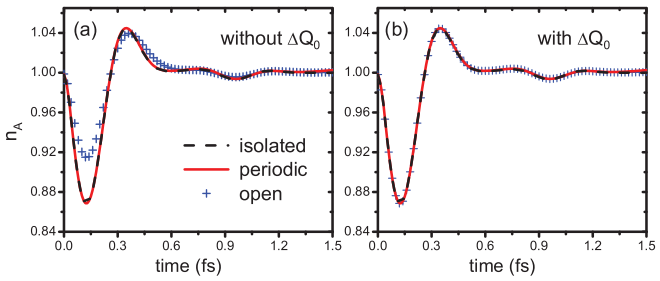

FIG. 3. (Color online) Time-dependent electron density on atom A (n_A) within the first 1.5 fs in response to a local potential shift. The three lines correspond to the isolated, periodic, and open boundary conditions, respectively. The calculation results obtained without and with the residual correction are presented in (a) and (b), respectively.

broadening of 10^{-2} eV adopted for the calculation of surface Green's functions.[73]

Although the equilibrium PDOS is reproduced with the fitted $\mathbf{\Lambda}(\epsilon)$, the minor fitting error of $\mathbf{\Lambda}(\epsilon)$ may affect the accuracy of the resulted real-time dynamics. To address this issue, we now look into the transient electronic dynamics on a graphene surface, as depicted in Fig. 1(b). We consider the scenario that the graphene is initially at equilibrium. At a certain time (set as $t = 0$), the on-site energy of atom A in the simulation box [see Fig. 1(b)] is shifted by 2 eV, which lasts for 0.05 fs and then vanishes. Experimentally this may be realized by applying a local voltage to an atom-sized gate electrode placed on top of the graphene. The time variation of electron density on the perturbed atom A, $n_A(t) = \boldsymbol{\sigma}_{AA}(t)$, is shown in Fig. 3(a). Within the first few femtoseconds, when the evolution of electronic response has not yet reached the boundary, the transient dynamics should be identical regardless of the specific boundary condition imposed.

In Fig. 3(a), the electronic dynamics under the open boundary condition is obtained by solving the HEOM of Eqs. (9)–(11). The resulting $n_A(t)$ exhibits some deviation from those of isolated and periodic models. The maximal deviation is observed at $t \sim 0.12$ fs. This thus exemplifies that the minor error in the Lorentzian fit of $\mathbf{\Lambda}(\epsilon)$ can lead to nontrivial error in the resulted real-time dynamics.

A residual correction approach has been proposed in Sec. II to minimize any possible error due to the insufficient accuracy of the Lorentzian fit. By applying the residual correction, the electronic dynamics for an open system is obtained by solving the HEOM consisting of Eqs. (11)–(13). As shown in Fig. 3(b), the deviation at $t \sim 0.12$ fs is completely eliminated. For all the numerical calculations we have carried out so far, the HEOM with the residual correction always guarantees quantitative agreement with the isolated or periodic model in the short-time transient regime. This is due to the fact that the external perturbation considered is not very strong, and hence the electronic dynamics involves only a relatively narrow energy range around the chemical potential of the environment.

Ideally, a more accurate decomposition scheme for $\mathbf{\Lambda}(\epsilon)$ is desired. A possible alternative approach to resolve the memory of the environment is to utilize the complex absorbing potential (CAP) method.[74–76] The CAP method imposes an optimized imaginary external potential on the environment, so that the decomposition of $\mathbf{\Lambda}(\epsilon)$ can be realized by analyzing the energetic

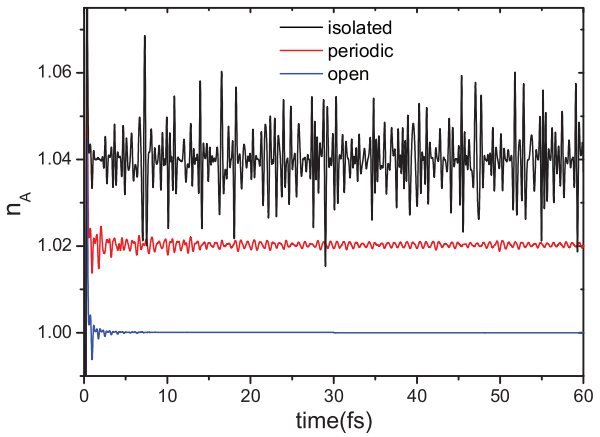

FIG. 4. (Color online) Time-dependent electron density on atom A (n_A) from $t = 0$ to 60 fs, in response to a local potential shift. The three lines correspond to the isolated, periodic, and open boundary conditions, respectively. For clarity, the data of isolated and periodic systems are elevated by 0.04 and 0.02, respectively.

structure of a finite region of environment, instead of using the Lorentzian fit of Eq. (6). The CAP method has been combined with the NEGF approach to study the time-dependent quantum transport problem in quasi-one-dimensional systems.[77,78] Note that the HEOM of Eqs. (9)–(11) can also be constructed based on a combined Padé decomposition and CAP scheme. This may further simplify the numerical procedures of the TDDFT-HEOM approach, which will be explored in our future work.

We then examine the long-time electronic response to the external perturbation, for which the boundary condition is expected to play a critical role. As displayed in Fig. 4, the long-time electronic dynamics for the three boundary conditions are distinctly different from each other. The isolated system exhibits a persistent fluctuation with a rather large amplitude. This is because the boundary is fully reflective. In contrast, with the periodic boundary the fluctuation retains a small but nonvanishing amplitude. This is because an electron leaving from one side of the box is forced to reenter at the counter side, and ultimately the electronic response is "evened" out inside the box. It is only with the open boundary that the fluctuation eventually damps out and the initial equilibrium is restored.

B. Real-time dynamics of an excess electron on a two-dimensional graphene surface

We now investigate the real-time dynamics of an excess electron on a graphene surface with the TDDFT-HEOM approach. Again, the graphene monolayer depicted in Fig. 1(b) is taken as the system. The graphene is initially in its equilibrium state. At a certain time (set as $t = 0$), an excess electron is injected onto atom A. Such a local perturbation drives the graphene out of equilibrium and induces electronic response that propagates outward from the perturbed site. Experimentally the single-electron injection may be realized with a tunneling junction setup.[79] The present scenario can be deemed as a quantum analog of "dripping a droplet into a

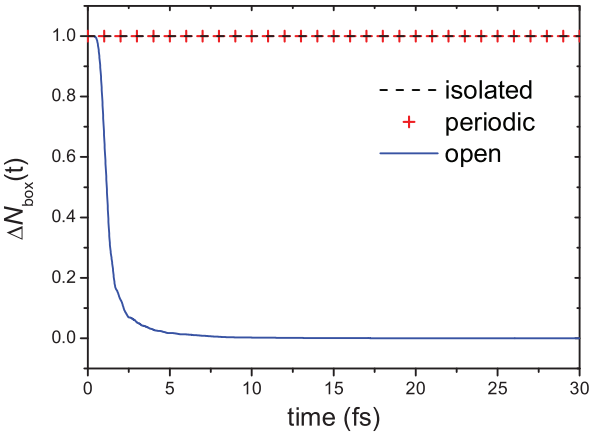

FIG. 5. (Color online) The number of excess electrons that remain within the simulation box vs time upon its injection onto atom A at $t = 0$.

liquid," which results in generation and spreading of electron ripples on the graphene surface.

Dissipation of an excess electron on the graphene plane is supposed to be one of the simplest examples of electronic dynamics on material surfaces. However, even such a simple case turns out to be rather challenging for conventional TDDFT. The major difficulty is that in reality the number of excess electrons remaining in the box, $\Delta N_{\rm box}(t) = \sum_{a\in{\rm box}} \sigma_{aa}(t) - \sigma^{\rm eq}_{aa}$, is not conserved as time goes on, whereas the isolated or periodic boundary condition forces it to be a constant; see Fig. 5. In contrast, the open-system TDDFT allows the excess electron to propagate through the (artificially designated) boundary and properly dissipate into the surrounding bulk graphene. A characteristic dissipation time τ_d can be defined as the time that $\Delta N_{\rm box}$ reduces to less than 0.01. From Fig. 5, we have $\tau_d = 6.6$ fs.

The simulation proceeds as follows. At $t = 0$ the electron occupation on atom A ($n_{\rm A} = \sigma_{\rm AA}$) increases instantaneously by 1, i.e., $n_{\rm A}(0^+) = n^{\rm eq}_{\rm A} + 1$. The subsequent real-time electronic dynamics are obtained by solving Eqs. (1)–(3) for isolated, periodic, and open boundary conditions, respectively. For simplicity the system is treated as spin-closed at any time.

We now examine how the electron density on atom A varies in time. The short-time evolution of $n_{\rm A}(t)$ is shown in Fig. 6(a). At $t < 1$ fs, the lines associated with the three types of boundary conditions overlap perfectly with each other.

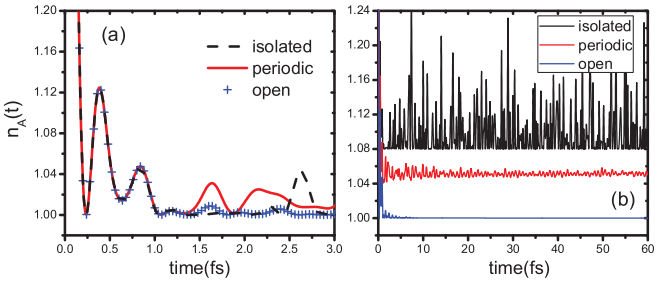

FIG. 6. (Color online) Time-dependent electron density on atom A ($n_{\rm A}$) from $t = 0$ to (a) 3 fs and to (b) 60 fs. For clarity, in (b) the data of isolated and periodic systems are elevated by 0.08 and 0.04, respectively.

Since the electronic dynamics should be identical before the first ripple wavefront reaches the boundary, such quantitative agreement verifies the accuracy of our proposed HEOM approach. Approximate schemes such as the wide-band limit[28] and complex absorbing potential[76,78,80] have been used for simplifying the evaluation of $\boldsymbol{Q}(t)$. The short-time transient dynamics presented here provides a potentially useful example for testing the accuracy of these approximate schemes.

Regarding the electronic response of graphene, a fundamental quantity is the time scale in which the ripples dissipate away so that the equilibrium is restored. To this end, the long-time electronic dynamics are displayed in Fig. 6(b). The figure looks very similar to Fig. 4. In the isolated model the electron density undergoes a significant and persistent fluctuation due to the fully reflective boundary, while in the periodic model the fluctuation retains a residual yet nonvanishing amplitude. Apparently, it is only with the open boundary that the fluctuation eventually damps out.

If one insists on using conventional TDDFT methods for isolated or periodic systems to study the real-time electronic response to a local perturbation, the size of the simulation box must be enlarged drastically to avoid the unwanted boundary effects. In practice, such calculations could be exceedingly costly, if not impossible.

The evolution of excess electron density, $\Delta n(\mathbf{r},t) = n(\mathbf{r},t) - n^{\rm eq}(\mathbf{r})$, is visualized in Fig. 7. For clarity the p_z atomic orbitals are represented by Gaussian functions. At $t = 0.5$ fs, when the propagation has not reached the boundary of the box, the three boundary conditions give the same pattern of ripples. The $\Delta n(\mathbf{r},t)$ exhibits a distinct threefold symmetry on the xy plane, reflecting the sp^2 bonding characteristics. At $t = 1.5$ fs, a significant portion of the excess electron should have dissipated into the surrounding graphene. Apparently, only the open-system model allows the excess electron to

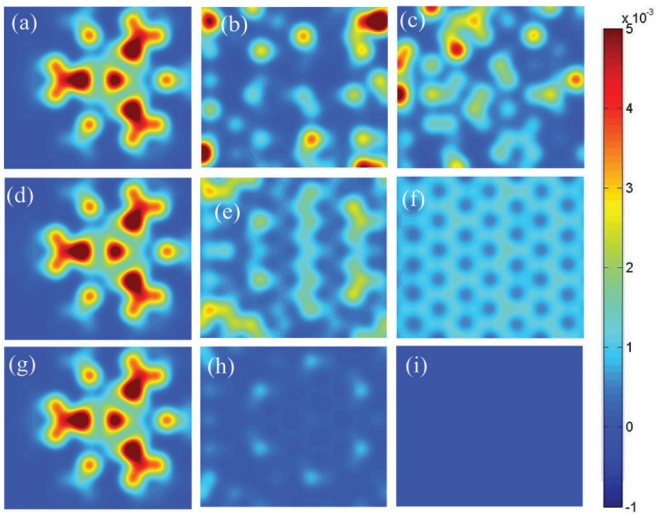

FIG. 7. (Color online) Snapshots of time-dependent density of excess electrons inside the simulation box, $\Delta n(\mathbf{r},t) = n(\mathbf{r},t) - n^{\rm eq}(\mathbf{r})$, after the excess electron is injected at $t = 0$. The upper, middle, and lower rows correspond to isolated, periodic, and open systems; and the left, middle, and right columns are for time instants $t = 0.5$, 1.5, and 20 fs, respectively. For a clear visualization, the p_z atomic orbitals are represented by Gaussian functions.

permeate through the boundary while preserving the threefold symmetry [see Fig. 7(h)]. In contrast, both the isolated and periodic models constrain the electron from leaving the box. At t as long as 20 fs, the ripples of the isolated model remain fluctuating, while the periodic boundary makes the excess electron "evenly" distributed among the sp^2 network. Only with the open-system model can the excess electron dissipate away properly.

C. Real-time electron transfer across a molecule-graphene interface

We now move to a more complex scenario in which a linear model molecule of four atoms is adsorbed on the graphene surface at atom B. TDDFT has been employed to study the ultrafast electron transfer in dye-sensitized solar cells with the isolated[81] and periodic[82,83] models. However, to the best of our knowledge, the boundary effects on the calculation results have not been explored.

The molecule assumes the same values of ϵ_0 and γ as the graphene, and their bonding strength is λ. At $t = 0$ an excess electron enters at the free end of the molecule, which drives the molecule-graphene composite out of equilibrium. Again, Eqs. (1)–(3) are used to simulate the real-time electronic dynamics subjected to the isolated, periodic, and open boundary conditions, respectively.

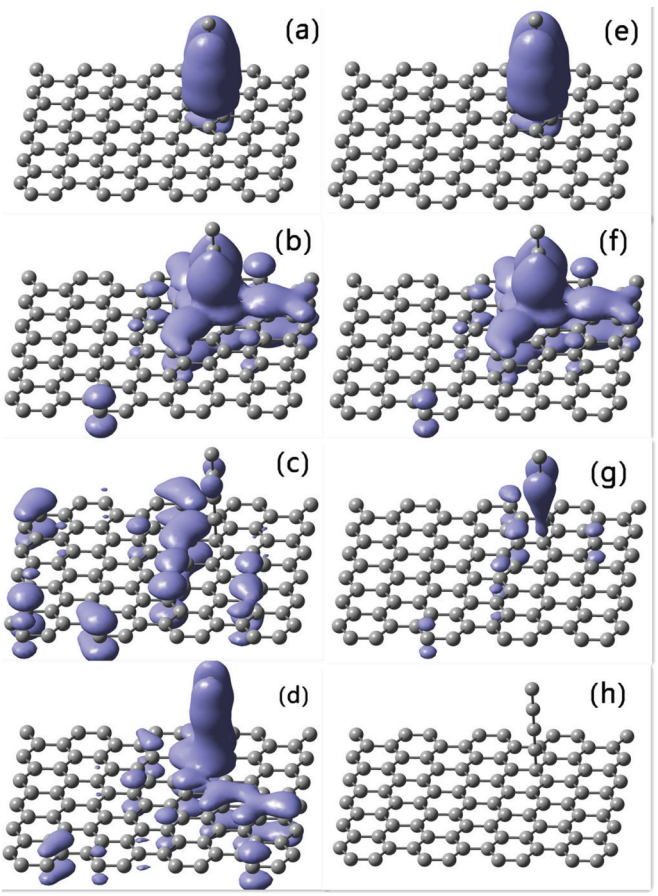

FIG. 8. (Color online) Isosurfaces of excess electron density $\Delta n(\mathbf{r},t) = 4 \times 10^{-4}$ bohr^{-3} for isolated (left column) and open (right column) system models at various time instants and $\lambda = \gamma = 2.7$ eV. The four rows from top to bottom are snapshots at $t = 0.5$, 1, 2.5, and 6.5 fs, respectively.

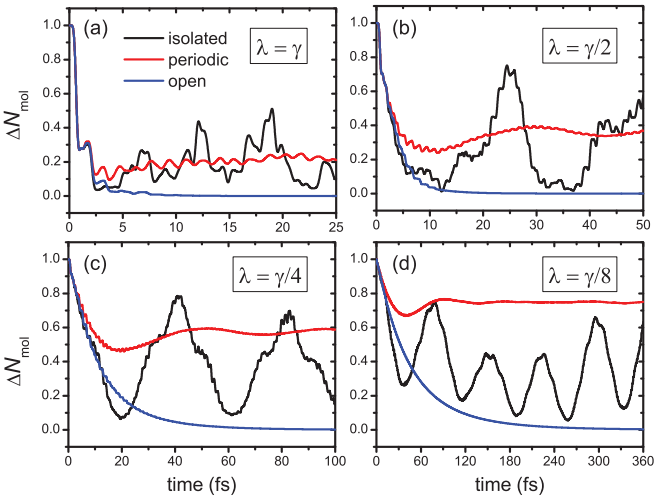

FIG. 9. (Color online) Number of excess electrons on the molecule vs time, $\Delta N_{\rm mol}(t)$, under the isolated, periodic, and open boundary conditions, respectively. The coupling strength between the molecule and the graphene is (a) $\lambda = \gamma$, (b) $\lambda = \gamma/2$, (c) $\lambda = \gamma/4$, and (d) $\lambda = \gamma/8$, respectively.

The evolution of the excess electron is displayed in Fig. 8 for $\lambda = \gamma$, where snapshots of the isolated boundary at various time instants are compared with the open-system counterparts. At $t < 1$ fs (the upper two rows), the dynamics occurs mostly inside the box, and both models give essentially the same result. In contrast, at $t > 2.5$ fs (the lower two rows) the dynamics become qualitatively different: in the isolated model the electron gets reflected at the boundary and sometimes repopulates on the molecule, while with the open boundary the excess electron gradually drains into the surrounding bulk graphene and vanishes entirely in the long-time limit.

Figure 9 plots the population of the excess electron on the molecule versus time, $\Delta N_{\rm mol}(t) = \sum_{a\in{\rm mol}} \sigma_{aa}(t) - \sigma^{\rm eq}_{aa}$, at various values of λ. Apparently, only with the open-system model the electron relaxation exhibits the correct long-time asymptotic behavior. A characteristic transfer time τ_t can be defined as the time that $\Delta N_{\rm mol}$ reduces to less than 0.01. From Fig. 9, τ_t is evaluated to be 7.6, 15.8, 66.5, and 270.5 fs for $\lambda/\gamma = 1$, 1/2, 1/4, and 1/8, respectively. This clearly infers that $\tau \propto 1/\lambda^2$, except at $\lambda = \gamma$ where the intramolecular dynamics is nearly in resonance with the interfacial electron transfer modes. While the isolated model gives reasonable short-time transient dynamics, at a long time the excess electron reappears on the molecule, which is clearly due to the artificial quantum confinement effect. In contrast, the periodic boundary withholds the electron from leaving the molecule, and this occurs even more so with a smaller λ. This stresses the fact that the periodic (or isolated) model lacks a relaxation channel in the absence of external fields and dissipative baths. Consequently, the excess electron is unable to lose energy to populate onto the low-lying graphene states.

IV. CONCLUDING REMARKS

To conclude, in this work we have improved the accuracy of a previously developed TDDFT-HEOM approach for open systems and extended its applicability to two-dimensional systems. The practicality and usefulness of the TDDFT-HEOM approach are exemplified with atomistic simulations of real-time electronic dynamics at a graphene surface and a molecule-graphene interface.

The real-time simulations highlight the significant role of the boundary condition in the electronic dynamics. Therefore, an open-system approach is particularly useful when the number of electrons within the region of primary interest is not conserved. As demonstrated in Sec. III, the TDDFT-HEOM approach is capable of characterizing accurately the exchange of electrons between a finite open system and its surrounding environment. Simulations of electronic dynamics on material surfaces may shed light on the mechanisms of some important interfacial processes, such as the electron transfer from (to) a bulk donor (acceptor) and reactions occurring on catalyst surfaces.

In the present work the TDDFT-HEOM approach is implemented with a tight-binding Hamiltonian. It is certainly desirable to go beyond this simple model and apply it at a first-principles level. To this end, an appropriate exchange-correlation functional form is needed to address the electron-electron interactions and possible excitonic effects. The influence of other dissipative sources, such as nuclear motions or phonon modes, can also be treated in the framework of TDDFT-HEOM. For instance, the effects of electron-phonon interactions on time-dependent quantum transport have been explored with the TDDFT-HEOM approach.[84] Further progress along this direction is underway.

ACKNOWLEDGMENTS

Support from the National Science Foundation of China (Grants No. 21103157, No. 21233007, No. 21322305, and No. 21303175), the Fundamental Research Funds for Central Universities (Grants No. 2340000034 and No. 2340000025), and the Strategic Priority Research Program (B) of the Chinese Academy of Sciences (Grant No. XDB01020000) is gratefully acknowledged. We thank Prof. GuanHua Chen and Prof. YiJing Yan for stimulating discussions.

*xz58@ustc.edu.cn

[1] B. O'Regan and M. Grätzel, Nature (London) **353**, 737 (1991).
[2] A. Hagfeldt and M. Grätzel, Acc. Chem. Res. **33**, 269 (2000).
[3] G. Li *et al*., Energy Environ. Sci. **2**, 230 (2009).
[4] E. Runge and E. K. U. Gross, Phys. Rev. Lett. **52**, 997 (1984).
[5] M. A. L. Marques and E. K. U. Gross, Annu. Rev. Phys. Chem. **55**, 427 (2004).
[6] K. Burke, J. Werschnik, and E. K. U. Gross, J. Chem. Phys. **123**, 062206 (2005).
[7] M. E. Casida and M. Huix-Rotllant, Annu. Rev. Phys. Chem. **63**, 287 (2012).
[8] M. E. Casida, in *Recent Developments and Applications of Modern Density Functional Theory*, edited by J. M. Seminario (Elsivier, Amsterdam, 1996), pp. 391–439.
[9] C. Y. Yam, S. Yokojima, and G. H. Chen, J. Chem. Phys. **119**, 8794 (2003).
[10] C. Y. Yam, S. Yokojima, and G. H. Chen, Phys. Rev. B **68**, 153105 (2003).
[11] R. van Leeuwen, Phys. Rev. Lett. **82**, 3863 (1999).
[12] R. van Leeuwen, in *Time-Dependent Density Functional Theory*, edited by M. A. L. Marques, C. A. Ullrich, F. Nogueira, A. Rubio, K. Burke, and E. K. U. Gross, Lecture Notes in Physics Vol. 706 (Springer-Verlag, Berlin, 2006), pp. 17–32.
[13] F. Kootstra, Ph.D. thesis, University of Groningen, 2001.
[14] N. T. Maitra, I. Souza, and K. Burke, Phys. Rev. B **68**, 045109 (2003).
[15] R. Baer, J. Chem. Phys. **128**, 044103 (2008).
[16] Y. Li and C. A. Ullrich, J. Chem. Phys. **129**, 044105 (2008).
[17] C. Verdozzi, Phys. Rev. Lett. **101**, 166401 (2008).
[18] *Fundamentals of Time-Dependent Density Functional Theory*, edited by M. A. L. Marques, N. T. Maitra, F. M. S. Nogueira, E. K. U. Gross, and A. Rubio, Lecture Notes in Physics Vol. 837 (Springer-Verlag, Berlin, 2012).
[19] S. Waidmann, M. Knupfer, B. Arnold, J. Fink, A. Fleszar, and W. Hanke, Phys. Rev. B **61**, 10149 (2000).
[20] V. Olevano and L. Reining, Phys. Rev. Lett. **86**, 5962 (2001).
[21] G. Onida, L. Reining, and A. Rubio, Rev. Mod. Phys. **74**, 601 (2002).
[22] S. Botti, A. Schindlmayr, R. D. Sole, and L. Reining, Rep. Prog. Phys. **70**, 357 (2007).
[23] G. Vignale and W. Kohn, Phys. Rev. Lett. **77**, 2037 (1996).
[24] N. Sai, M. Zwolak, G. Vignale, and M. Di Ventra, Phys. Rev. Lett. **94**, 186810 (2005).
[25] D. S. Kosov, J. Chem. Phys. **119**, 1 (2003).
[26] S. Kurth, G. Stefanucci, C.-O. Almbladh, A. Rubio, and E. K. U. Gross, Phys. Rev. B **72**, 035308 (2005).
[27] K. Burke, R. Car, and R. Gebauer, Phys. Rev. Lett. **94**, 146803 (2005).
[28] X. Zheng, F. Wang, C. Y. Yam, Y. Mo, and G. H. Chen, Phys. Rev. B **75**, 195127 (2007).
[29] X. Q. Li and Y. J. Yan, Phys. Rev. B **75**, 075114 (2007).
[30] G. Stefanucci and C.-O. Almbladh, Europhys. Lett. **67**, 14 (2004).
[31] M. Di Ventra and T. N. Todorov, J. Phys.: Condens. Matter **16**, 8025 (2004).
[32] X. Zheng and G. H. Chen, arXiv:physics/0502021.
[33] X. Zheng, C. Y. Yam, F. Wang, and G. H. Chen, Phys. Chem. Chem. Phys. **13**, 14358 (2011).
[34] J. Yuen-Zhou, D. G. Tempel, C. A. Rodríguez-Rosario, and A. Aspuru-Guzik, Phys. Rev. Lett. **104**, 043001 (2010).
[35] D. G. Tempel, M. A. Watson, R. Olivares-Amaya, and A. Aspuru-Guzik, J. Chem. Phys. **134**, 074116 (2011).
[36] G. Stefanucci and C.-O. Almbladh, Phys. Rev. B **69**, 195318 (2004).
[37] C. Y. Yam *et al*., Nanotechnology **19**, 495203 (2008).
[38] G. Stefanucci, E. Perfetto, and M. Cini, Phys. Rev. B **81**, 115446 (2010).
[39] Y. Xing, B. Wang, and J. Wang, Phys. Rev. B **82**, 205112 (2010).

[40]S.-H. Ke, R. Liu, W. Yang, and H. U. Baranger, J. Chem. Phys. **132**, 234105 (2010).
[41]S. Z. Wen *et al*., J. Phys. Chem. B **115**, 5519 (2011).
[42]A. Castro *et al*., Phys. Status Solidi B **243**, 2465 (2006).
[43]Y. Zhu, J. Maciejko, T. Ji, H. Guo, and J. Wang, Phys. Rev. B **71**, 075317 (2005).
[44]P. Cui, X. Q. Li, J. S. Shao, and Y. J. Yan, Phys. Lett. A **357**, 449 (2006).
[45]J. S. Jin, X. Zheng, and Y. J. Yan, J. Chem. Phys. **128**, 234703 (2008).
[46]X. Zheng, J. S. Jin, S. Welack, M. Luo, and Y. J. Yan, J. Chem. Phys. **130**, 164708 (2009).
[47]X. Zheng *et al*., Prog. Chem. **24**, 1129 (2012).
[48]X. Zheng, J. S. Jin, and Y. J. Yan, J. Chem. Phys. **129**, 184112 (2008).
[49]X. Zheng, J. S. Jin, and Y. J. Yan, New J. Phys. **10**, 093016 (2008).
[50]X. Zheng, J. Y. Luo, J. S. Jin, and Y. J. Yan, J. Chem. Phys. **130**, 124508 (2009).
[51]Z. H. Li, N. H. Tong, X. Zheng, D. Hou, J. H. Wei, J. Hu, and Y. J. Yan, Phys. Rev. Lett. **109**, 266403 (2012).
[52]X. Zheng, Y. J. Yan, and M. Di Ventra, Phys. Rev. Lett. **111**, 086601 (2013).
[53]S. Wang, X. Zheng, J. S. Jin, and Y. J. Yan, Phys. Rev. B **88**, 035129 (2013).
[54]J. Maciejko, J. Wang, and H. Guo, Phys. Rev. B **74**, 085324 (2006).
[55]X. Zheng *et al*., J. Chem. Phys. **133**, 114101 (2010).
[56]H. Xie *et al*., J. Chem. Phys. **137**, 044113 (2012).
[57]H. Tian and G. H. Chen, J. Chem. Phys. **137**, 204114 (2012).
[58]Y. Zhang, S. G. Chen, and G. H. Chen, Phys. Rev. B **87**, 085110 (2013).
[59]A. Croy and U. Saalmann, Phys. Rev. B **80**, 245311 (2009).
[60]L. V. Keldysh, JETP **20**, 1018 (1965).
[61]D. C. Langreth and P. Nordlander, Phys. Rev. B **43**, 2541 (1991).
[62]A. Croy and U. Saalmann, Phys. Rev. B **80**, 073102 (2009).
[63]T. Ozaki, Phys. Rev. B **75**, 035123 (2007).
[64]J. Hu, R. X. Xu, and Y. J. Yan, J. Chem. Phys. **133**, 101106 (2010).
[65]J. Hu, M. Luo, F. Jiang, R. X. Xu, and Y. J. Yan, J. Chem. Phys. **134**, 244106 (2011).
[66]S. Datta, *Electronic Transport in Mesoscopic Systems* (Oxford University Press, New York, 1995).
[67]J. Taylor, H. Guo, and J. Wang, Phys. Rev. B **63**, 245407 (2001).
[68]J. S. Toll, Phys. Rev. **104**, 1760 (1956).
[69]M. P. López Sancho, J. M. López Sancho, and J. Rubio, J. Phys. F **15**, 851 (1985).
[70]D. W. Boukhvalov, M. I. Katsnelson, and A. I. Lichtenstein, Phys. Rev. B **77**, 035427 (2008).
[71]R. N. Sajjad, C. Polanco, and A. W. Ghosh, J. Comput. Electron. **12**, 232 (2013).
[72]A. C. Neto, F. Guinea, N. Peres, K. Novoselov, and A. Geim, Rev. Mod. Phys. **81**, 109 (2009).
[73]X. Zheng, S.-H. Ke, and W. Yang, J. Chem. Phys. **132**, 114703 (2010).
[74]R. Kosloff and D. Kosloff, J. Comput. Phys. **63**, 363 (1986).
[75]D. E. Manolopoulos, J. Chem. Phys. **117**, 9552 (2002).
[76]R. Baer, T. Seideman, S. Ilani, and D. Neuhauser, J. Chem. Phys. **120**, 3387 (2004).
[77]J. A. Driscoll and K. Varga, Phys. Rev. B **78**, 245118 (2008).
[78]L. Zhang, J. Chen, and J. Wang, Phys. Rev. B **87**, 205401 (2013).
[79]G. Fève *et al*., Science **316**, 1169 (2007).
[80]K. Varga, Phys. Rev. B **83**, 195130 (2011).
[81]Z. Guo, W. Liang, Y. Zhao, and G. H. Chen, J. Phys. Chem. C **112**, 16655 (2008).
[82]W. R. Duncan, C. F. Craig, and O. V. Prezhdo, J. Am. Chem. Soc. **129**, 8528 (2007).
[83]S. Meng, J. Ren, and E. Kaxiras, Nano. Lett. **8**, 3266 (2008).
[84]Y. Zhang, C. Y. Yam, and G. H. Chen, J. Chem. Phys. **138**, 164121 (2013).